```
@article{sandoval2024abort,
  author = {Sergio A. Sandoval and Ping Lu and John T. Hwang},
  title = {Abort Guidance During Lunar Powered Descent},
  journal = {Journal of Guidance, Control, and Dynamics},
  year = {2024},
  volume = {47},
  number = {3},
  pages = {394-406},
  doi = {10.2514/1.g007086},
  url = {https://doi.org/10.2514/1.g007086}
}
```

Abort Guidance during Lunar Powered Descent

Sergio A. Sandoval * and Ping Lu†
San Diego State University, San Diego, CA 92182

John T. Hwang‡
University of California, San Diego, CA 92093

During powered descent of a crewed lunar landing mission, the ability to abort and ascend into a clear pericynthion orbit is critical in case any contingency renders the landing infeasible or excessively risky. In such a case it is incumbent upon the guidance system to determine autonomously a safe abort trajectory and the associated guidance command. To accomplish this task reliably, a novel two-phase abort guidance strategy is proposed in this paper where a pull-up maneuver redirects the velocity vector to help mitigate any ground collision risk and achieve an appropriate initial ascent condition, followed by a fuel-optimal ascent guidance algorithm to insert the spacecraft into a predefined safe orbit around the Moon. Development of the pull-up guidance laws and a description of the fuel-optimal ascent guidance based on the indirect method of optimal control are presented. In-depth investigation is conducted to provide a full understanding on the validity of the abort solutions. The solutions and fuel efficiency of the proposed guidance strategy are independently verified by using a direct method of optimal control. Monte Carlo closed-loop simulations demonstrate the effectiveness and robustness of this method throughout the entire powered descent.

Author version · cite the published paper: doi.org/10.2514/1.g007086

I. Introduction

In a crewed space mission the ability to abort throughout all the mission phases has been an important requirement since the Apollo program.[1] For a crewed lunar landing mission a particularly challenging phase for abort is in powered descent. In powered descent the abort would be for the lander to stop descent, turn around, and ascend into a pericynthion orbit clear of any mountains on the Moon, and then rendezvous with the rescue spacecraft.[1, 2] It is particularly challenging because abort in this phase necessitates aggressive maneuvers that in most cases must reverse the direction of the vertical motion before the abort, and insertion into the specified orbit must be reliably achieved from a wide range of possible initial conditions that are likely far from a typical initial condition for ascent flight.

In the Apollo program the Apollo Primary Guidance Navigation and Control System (PGNCS) was used to fly the

*Graduate Research Assistant, Department of Aerospace Engineering; ssandoval4327@sdsu.edu, Student Member AIAA
†Professor and Chair, Department of Aerospace Engineering; plu@sdsu.edu, Fellow AIAA
‡Assistant Professor, Department of Mechanical and Aerospace Engineering; jhwang@eng.ucsd.edu, Member AIAA

Lunar Module (LM) during descent, ascent, aborts, and rendezvous. There were two descent abort guidance programs, P70 for abort using the descent stage engine, and P71 if the ascent stage propulsion system is required to achieve orbit insertion. The targeted orbital insertion conditions were different depending on where the abort would take place during descent, because of the varying relative position between the LM and Command and Service Module (CSM) - which stayed on the lunar orbit - and the rendezvous requirement with CSM after abort.[3] For aborts during descent, the PGNCS would fly the vehicle using the same guidance law and logic for lunar ascent. The guidance system commands only attitude, and no engine throttling is used. The abort guidance begins with the attitude pitched to the vertical, similar to the vertical rise phase in ascent from the lunar surface, until the altitude is greater than 25,000 ft (for nominal lunar ascent the vertical rise terminates when the altitude rate reaches +40 ft/s). During the vertical rise the LM is rotated to the desired azimuth (normally in the CSM orbital plane). The next phase, orbit insertion phase, is designed for efficient propellant usage to achieve the targeting condition.[3] The guidance command is defined by an acceleration profile which is a linear function of time. The time-to-go is determined by the velocity to be gained. Based on the current state and the targeting condition, the guidance law determines the accelerations in the radial and crossrange directions.[3]

In the event of a PGNCS failure during descent, the landing would not be attempted. The backup system, the Abort Guidance System (AGS), would be used to insert the LM into a safe orbit and accomplish the rendezvous with the CSM. The AGS was not designed to support lunar landing. The early back-up powered-descent abort plans were complex because of the limited onboard capabilities in navigation, computation, guidance, and communication.[1] An early version of the AGS was to provide a pitch sequence based on the time of abort and stored constants and produces a thrust cut-off signal based on the velocity.[2] A compensation scheme compared velocity readings from an accelerometer on the thrust axis with nominal velocity values at specified time intervals, and adjusted pitch attitude and velocity at engine cut-off.[2] Later as a general-purpose computer TRW MARCO 4418 became available onboard, this open-loop guidance plus closed-loop compensation design of AGS was abandoned in favor of a simplified explicit ascent guidance algorithm.[4] According to Goodman,[4] the AGS guidance algorithm is similar to that reported in Ref. [5]. The guidance method in Ref. [5] targets a particular set of final conditions specified by the final radius and radial velocity as well as crossrange. The engine cut-off time is chosen to meet the targeting value of the total final velocity.

The lander of the next crewed lunar mission will have modern avionics and flight computers with capabilities far exceeding what was available in the Apollo program. To the best of our knowledge, there has not been published systematic work since the Apollo program on abort during the powered descent of a lunar landing mission. The planned return to the Moon by astronauts in NASA's Artemis Program renders such an effort necessary and timely. The goal of this work is to take advantage of the advance in onboard computational capabilities to develop a fully automated and streamlined (as compared to Apollo abort guidance) powered-descent abort guidance method and algorithm that can autonomously steer the vehicle to safely insert into the specified pericynthion orbit, from abort at any point on the powered descent trajectory where it is still physically feasible to abort by the lander. To be adaptive to any feasible abort condition and targeting condition, and ensure high reliability, the guidance system should be able to successfully guide the vehicle to achieve the target orbit, without relying on any pre-calculated guidance data or reference values. The guidance strategy should be safe, accurate, and as simple as possible. Another potentially critical limiting factor that can impact adversely the success in powered-descent abort is excessive propellant usage. Therefore we shall further require that the ascent guidance be optimal in the sense of using the least amount of propellant.

In an abort scenario, the first instinct is to start the ascent towards a safe orbit immediately, regardless of the current state of the vehicle. This belief stems from the idea that an instantaneous evacuation of the vehicle is necessary to keep astronauts safe. However, it is important to recognize that the conditions of the vehicle during powered descent can render starting the abort ascent immediately a potentially risky proposition, especially late in descent, where the danger of colliding with the ground exists. We will demonstrate such possibilities through investigation in this paper.

To ensure safe and fuel-efficient abort, an automated two-phase powered-descent-abort guidance strategy is developed in this work.[6] The first phase is a pull-up phase where the vehicle maneuvers to stop descending and achieve a initial favorable state for ascent that assures ground clearance during ascent. The second phase is fuel-optimal ascent into the specified orbit. This guidance strategy and the target pericynthion orbit remain the same for abort throughout the entire powered descent trajectory, greatly simplifying the implementation and guidance logic. Figure 1 illustrates the concept of operations for this powered-descent-abort strategy.

The fuel-optimal guidance is performed by the algorithm in Ref. [7], dubbed Universal Powered Guidance for Ascent (UPG+A). It is an indirect-method based algorithm that solves the 3-dimensional fuel-optimal ascent problem quickly and reliably. To allow flexibility in the orbital insertion point of the abort ascent, depending on the condition of abort along the powered descent trajectory, the deployed orbital insertion constraints only specify the shape, size and orientation of the pericynthion orbit, but not the actual insertion point into the orbit (sometimes known as “free-attachment-point"). This freedom however produces a phenomenon that there may be two local optimal solutions for the fuel-optimal ascent problem.[8] In this work this issue is carefully investigated to provide a clear understanding that the abort ascent trajectory by the proposed guidance strategy is always safe and satisfies accurately the orbital insertion requirements.

In the rest of this paper, the abort guidance problem during powered descent is formulated; the two-phase abort guidance strategy is supported by the development of fuel-efficient pull-up guidance laws, and introduction of the fuel-optimal ascent guidance algorithm. The fuel-optimal ascent solution is carefully analyzed to gain a full understanding, and its validity is verified by an independent direct method. End-to-end Monte Carlo simulations for abort throughout the powered descent trajectory for a lunar landing mission at the South Pole of the Moon are provided to demonstrate the robustness and effectiveness of the guidance approach.

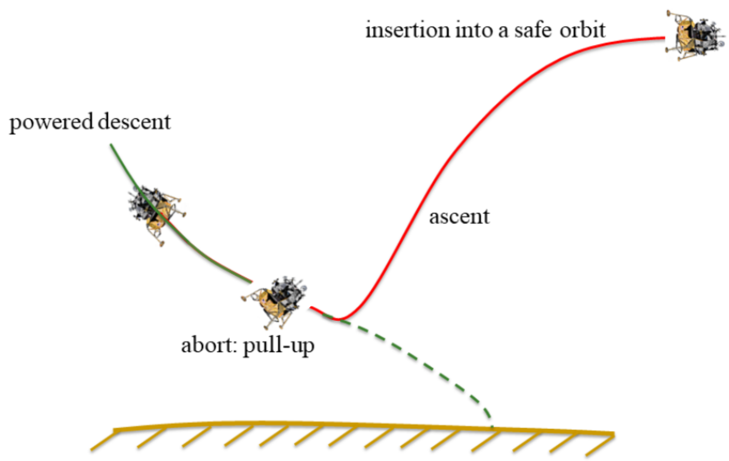

Fig. 1 Concept of Operations for two-phase abort strategy during lunar powered descent

II. Guidance Problem

In a Cartesian coordinate system with the origin at the center of the Moon, the three-dimensional point-mass equations of motion for a rocket-powered vehicle can be written as

$$\dot{\boldsymbol{r}} = \boldsymbol{V} \tag{1}$$

$$\dot{\boldsymbol{V}} = \boldsymbol{g}(\boldsymbol{r}) + \frac{T}{m(t)}\mathbf{1}_T(t) \tag{2}$$

$$\dot{m} = -\frac{T}{v_{ex}} \tag{3}$$

$$0 \le T(t) \le T_{max} \tag{4}$$

The rocket engine thrust has a magnitude T and $\mathbf{1}_T$ is the *unit* vector that defines the thrust direction. The direction of $\mathbf{1}_T$ generally changes with time, and T is allowed to vary as well, subject to the prescribed upper bound limit T_{max}. The effective exhaust velocity of the rocket engine v_{ex} is considered a constant. The vectors $\boldsymbol{r} \in R^3$ and $\boldsymbol{V} \in R^3$ are the position and velocity vector of the vehicle with the current mass m. To capture the effects of the changing direction of the gravitational force in problems with relatively long flight distances, a central gravitational acceleration model $\boldsymbol{g} = -\mu\boldsymbol{r}/R_0^3$ is used where μ is the gravitational parameter of the Moon, and R_0 is the equatorial radius of the Moon. Clearly this is an approximation to the Newtonian gravity $\boldsymbol{g} = -\mu\boldsymbol{r}/\|\boldsymbol{r}\|^3$. This approximation preserves the varying direction of the gravity, but carries a small discrepancy in the magnitude. In the ascent guidance problem the changing direction of the gravity has a much more pronounced effect on the solution than the variations in the magnitude of gravitational acceleration. This “linear gravity" model works well in capturing the more important variations.

The powered guidance problem is to determine $\mathbf{1}_T$, T and the burn time to meet the required targeting condition and optimized a performance index when applicable.

III. Nominal Crewed Lunar Landing Mission

A nominal crewed lunar landing trajectory is used as the baseline for abort guidance investigation. The vehicle and mission characteristics are similar to those from the Apollo LM and the Apollo 11 mission [3], except that the target landing site is at the South Pole of the Moon.[9] The LM consists of a descent stage and ascent stage - see Fig. 2. In this paper, the descent propulsion system (DPS) is assumed to be healthy and available for an abort. The guidance abort approach described in this paper however is also applicable to an abort where the ascent stage propulsion is required as well for insertion into the target orbit. The combined fuel in the descent and ascent stages is assumed to be available for abort in assessing abort feasibility. The descent stage engine of the LM has a maximum thrust of 45,000 N and a specific impulse of 311 sec. The descent condition starts at the perilune of a 60 nm x 50,000 ft descent orbit.[3] The complete set of initial conditions are given in Table 1. [9] All the 3DOF simulation results in this section are obtained by closed-loop simulations where the guidance commands are updated at a rate of 2 Hz. The Moon is modeled as an ellipsoid and self-rotation of the Moon is considered. Perfect navigation information is assumed. Figure 3 shows the ground track of the landing trajectory from the perilune of the descent orbit to touchdown at the South Pole.

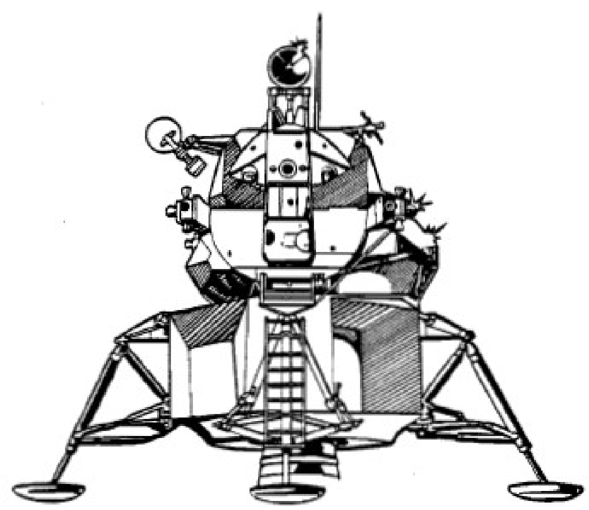

Fig. 2 Apollo Lunar Landing Module

The powered descent is guided by a fractional-polynomial powered descent guidance (FP^{2}DG) law [10]. The family of FP^{2}DG laws is a recent discovery, and the venerable Apollo lunar descent guidance law [11] and Apollo era E-guidance [12] law are shown to be two members of the FP^{2}DG family [10]. Figure 4 shows the profiles of several trajectory parameters along the nominal powered descent trajectory [10]. The powered descent lasts 620 seconds. After 400 seconds in powered descent, the flight path angle (fpa) rapidly decreases toward -90 deg, which increases the difficulty in performing a safe abort.

Table 1 Mission initial conditions and vehicle data

Perilune Condition	Value
altitude (km)	15.24
longitude (deg)	41.85
latitude (deg)	-71.6
inertial velocity (m/s)	1,698.3
inertial topocentric flight path angle (deg)	0.0
inertial topocentric azimuth angle (deg)	180
downrange (km)	559.41
crossrange (km)	0.48
total vehicle mass (kg)	15,103
total fuel mass (kg)*	10,624
vehicle dry mass (kg)†	4,479

[a]Including the propellant and oxidizer in descent and ascent stages.

[b]The sum of the dry masses of the descent and ascent stages.

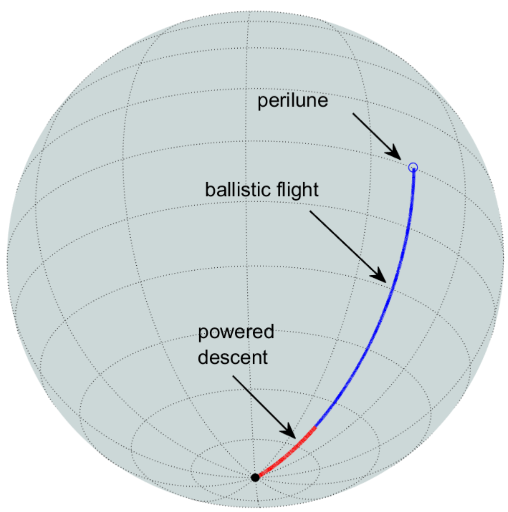

Fig. 3 Nominal ground track for landing at the South Pole of the Moon

IV. Direct Abort

When it becomes necessarily to abort the landing mission, the lander is to fly into a 10 km × 150 km pericynthion orbit at an inclination of 90 deg. The perilune altitude of 10 km of this orbit will clear off any mountains on the Moon.[2] The apolune altitude and inclination may be determined by the phasing and rendezvous considerations with respect to the Command Module after the abort. In an abort scenario, the thrust magnitude T is always at full throttle, $T(t) = T_{max}$. Hence, the only control available is the thrust direction vector $\mathbf{1}_T(t)$, changing with time. In this section

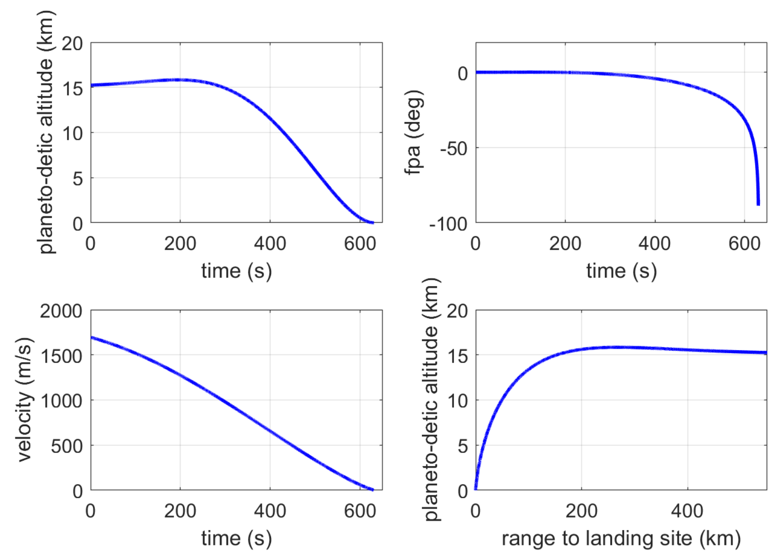

Fig. 4 Nominal Powered Descent Trajectory for a Landing at the South Pole of the Moon

we briefly investigate the viability of the strategy of immediately commanding ascent to the target pericynthion orbit from the powered descent trajectory by an optimal guidance algorithm, as soon as abort is commenced.

A. Optimal Ascent Guidance

Ascent guidance in this paper is accomplished by the UPG+A algorithm [7]. In this subsection UPG+A is briefly reviewed. The reader is referred to Ref. [7] and Ref. [13] for algorithmic details. UPG+A solves the optimal control problem subject to the dynamics in Eqs. (1)–(3) and with a performance index of minimizing the propellant consumption

$$J = \int_{t_0}^{t_f} [-T(t)/v_{ex}]\, dt = m(t_f) - m(t_0) \tag{5}$$

where t_0 is the time when the ascent phase starts, and t_f is free. Since the thrust T is fixed at the maximum value, the propellant-optimal problem is the same as the time-optimal problem. While UPG+A allows any combinations of orbital insertion conditions, the final constraints for the optimal abort-ascent problem are the orbital insertion conditions into the target abort orbit specified by the given semi-major axis a^*, eccentricity $e^* \neq 0$, and orbital inclination $i^* \neq 0$. In terms of the final radius and velocity vectors $\boldsymbol{r}_f = \boldsymbol{r}(t_f)$ and $\boldsymbol{V}_f = \boldsymbol{V}(t_f)$ at the engine cut-off time t_f, the terminal constraints on these 3 orbital elements may be expressed in the following form:

$$(\boldsymbol{r}_f \times \boldsymbol{V}_f)^T(\boldsymbol{r}_f \times \boldsymbol{V}_f) - \mu a^*(1 - e^{*2}) = 0 \tag{6}$$

$$V_f^2/2 - \mu/r_f + \mu/2a^* = 0 \tag{7}$$

$$\mathbf{1}_z^T(\boldsymbol{r}_f \times \boldsymbol{V}_f) - \|\boldsymbol{r}_f \times \boldsymbol{V}_f\| \cos i^* = 0 \tag{8}$$

where $r_f = \|\boldsymbol{r}_f\|$, $V_f = \|\boldsymbol{V}_f\|$, and $\mathbf{1}_z$ is a unit vector parallel to the polar axis of the Moon (pointing to the North). Note that the insertion point into the specified orbit is not constrained (not at a particular point of the orbit, e.g., the perilune), but is left for the guidance algorithm to optimize. This is a so-called free-attachment-point case. Not limiting the orbital insertion to occur at a particular point leaves much welcomed flexibility for the ascent trajectory in the already highly stressful situation in a powered-descent-abort. Depending on when abort happens during powered descent, the freedom to insert into the specified orbit at a most suitable point for the case is important, as will be seen later.

Among the 6 classical orbital elements, the 3 that are free in this case are the argument of perilune, longitude of the ascending node, and true anomaly at insertion. The necessary conditions of the optimal control problem call for 6 transversality conditions on $\boldsymbol{p}_{V_f}$ and $\boldsymbol{p}_{r_f}$, the velocity and radius costate vectors at the final time [14]. The elimination of the 3 Lagrange multipliers associated with the constraints in Eqs. (6)–(8) in the transversality conditions will lead to 3 independent *reduced transversality conditions* as follows [15]:

$$(\boldsymbol{p}_{r_f} \times \boldsymbol{r}_f + \boldsymbol{p}_{V_f} \times \boldsymbol{V}_f)^T(\boldsymbol{r}_f \times \boldsymbol{V}_f) = 0 \tag{9}$$

$$(\boldsymbol{p}_{r_f} \times \boldsymbol{r}_f + \boldsymbol{p}_{V_f} \times \boldsymbol{V}_f)^T\mathbf{1}_z = 0 \tag{10}$$

$$\boldsymbol{p}_{r_f}^T\boldsymbol{V}_f - \frac{\mu}{r_f^3}\boldsymbol{p}_{V_f}^T\boldsymbol{r}_f = 0 \tag{11}$$

The last condition is from the transversality condition on the Hamiltonian at t_f for free-time optimal control problems[7]:

$$\boldsymbol{p}_{r_f}^T\boldsymbol{V}_f - \mu\boldsymbol{p}_{V_f}^T\boldsymbol{r}_f + T_{max}\|\boldsymbol{p}_{V_f}\|/m(t_f) - 1 = 0 \tag{12}$$

In UPG+A, the costate vectors $\boldsymbol{p}_r(t)$ and $\boldsymbol{p}_V(t)$ have closed-form solutions as functions of time t and the initial costate $\boldsymbol{p}_{r_0}$ and $\boldsymbol{p}_{V_0}$. With the given initial state at t_0 and a piecewise-constant thrust profile (in this case it is all constant) the solution to the state equations can also be approximated by numerical quadratures in closed form as the functions of $\boldsymbol{p}_{r_0}$ and $\boldsymbol{p}_{V_0}$. See Refs. [7] and [13] for detail. The two-point-boundary-value problem from the necessary conditions of the optimal control problem then reduces to a root-finding problem where the 7 unknowns $\boldsymbol{p}_{r_0}$, $\boldsymbol{p}_{V_0}$ and t_f are found to meet Eqs. (6)–(12). UPG+A solves this zero-finding problem problem quickly and reliably by using a step-size controlled

Newton-Raphson method. The solution provides the optimal command for $\mathbf{1}_T(t)$ at the current time t as

$$\mathbf{1}_T(t) = \boldsymbol{p}_V(t)/\|\boldsymbol{p}_V(t)\| \tag{13}$$

In the next guidance cycle, the problem is resolved with the actual trajectory state at the time as the initial condition, and the updated command for $\mathbf{1}_T$ and the time-to-insertion are obtained. In this way, closed-loop ascent guidance is effectively achieved by UPG+A. The orbital insertion conditions are typically attained with high accuracy by the guidance (thus there is no need for targeting error budget for guidance).

In a case where the ascent stage propulsion is required for orbital insertion, after the use of the descent stage propulsion, the fuel-optimal ascent problem is effectively a two-stage ascent problem, and UPG+A can readily accommodate the need.[7]

It should be noted that even though UPG+A is used for descent-abort guidance in this paper, the same algorithm/software is well suited for nominal lunar ascent. Hence no added cost or software complexity would incur associated with using the same software for abort guidance if it is already implemented for lunar ascent. Furthermore, since the algorithm is model based, the same software/program would be used regardless of whether the abort is performed with the descent-stage engine or ascent-stage engine.

B. Direct Abort Solutions

During the powered descent, at any particular instant when abort is commenced, UPG+A is deployed immediately to guide the lander to ascend to the target orbit. In Fig. 5 a number of closed-loop guided ascent trajectories are plotted that correspond to aborts at different times after Powered Descent Initiation (PDI) which signifies the start of the powered descent. These abort instants are at a 100-sec increment after PDI until 600 sec after PDI. Notice that the ascent trajectories until around 300 seconds after PDI insert into the target orbit at a higher altitude than the perilune altitude (about 12 km in geodetic altitude). This is a manifestation of the fact that UPG+A finds the optimal insertion altitude to take advantage of free-attachment-point in the orbital insertion conditions. After 300 sec since PDI, the abort ascent trajectories all enter the target orbit at the perilune, again optimal in these cases.

To show the validity of the solutions by UPG+A, the optimal ascent trajectories by UPG+A are verified by an independent software named OpenMDAO.[16] OpenMDAO is an open-source optimization framework and a platform to building new analysis tools for faster, more stable design optimization with tight integration of high-fidelity analyses into system level models. A functionality of OpenMDAO is to solve the trajectory optimization problem by the direct method.

The same abort-ascent problems at different times since PDI are also solved by OpenMDAO to minimize the fuel consumption (or equivalently, the flight time). Plotted in Fig 5 in green dashed line are also the *open-loop* ascent trajectories obtained by OpenMDAO. In all but one case the trajectories are practically the same in the scale of the figure. The only case where some relative small differences are visible is the case of abort at 600 sec since PDI. This is the latest abort among all the cases (and the most challenging one). Still, considering that the UPG+A trajectory is the result of closed-loop simulation, and the solution by OpenMDAO is an open-loop trajectory, the differences are quite reasonable. Table 2 compares the propellant consumption between the two groups of the trajectories. The differences are in the range of $0.1\% - 1.7\%$. Again these small discrepancies can be attributed predominantly to the differences between the closed-loop simulated trajectories under UPG+A and open-loop solutions from OpenMDAO.

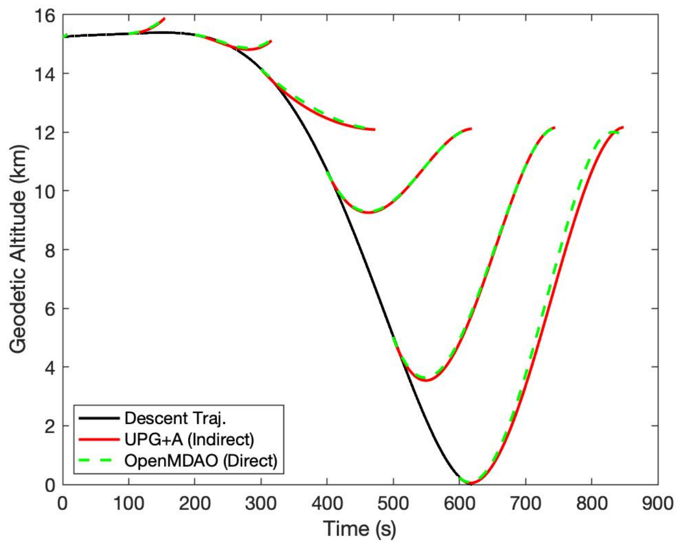

Fig. 5 Ascent trajectories during lunar powered descent from closed-loop simulations guided by UPG+A and open-loop solutions from OpenMDAO

Table 2 Propellant Consumption Comparison between UPG+A guided solutions and OpenMDAO solutions

Abort Time since PDI (sec)	Propellant Consumption (kg)	
	UPG+A guided	OpenMDAO
100	808.58	823.21
200	1709.74	1723.94
300	2546.47	2556.99
400	3224.36	3234.16
500	3619.76	3623.54
600	3665.82	3681.30

So far the tests seem to suggest that direct abort is viable. But a closer examination of the ascent trajectories in late abort cases reveals a critical issue: the ascent trajectories in some late abort cases risk to collide with the lunar surface before ascending to the orbit. This problem can get significantly worse if abort takes place further late into the powered descent. Figure 6 zooms in the final portion of the powered descent phase and illustrates several direct abort trajectories from 580 sec to 620 sec since PDI. It can be seen that some of the abort-ascent trajectories indeed intersect the ground.

To eliminate the risk of colliding with the lunar surface in abort, a ground clearance constraint may be imposed in UPG+A. But this will significantly complicate the algorithm and adversely affect its robustness. A simpler, fail-safe, and propellant-efficient strategy is necessary to pull the lander out of descent and enable fuel-optimal ascent into the target orbit. Such a necessity motivates the two-phase guidance strategy developed in the next section.

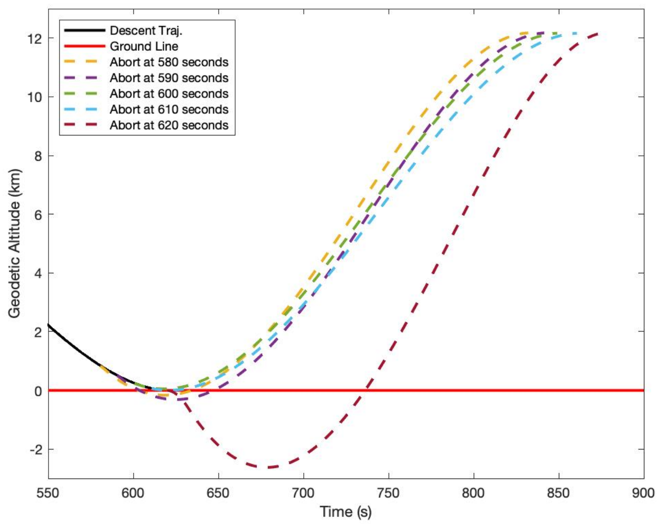

Fig. 6 Late Abort Solutions using Single-Phase Abort

V. Two-Phase Abort Guidance Strategy

To ensure a safe and propellant efficient abort trajectory once abort is commanded during lunar powered descent, a two-phase abort strategy is proposed. The abort problem is separated in two phases: a pull-up maneuver and an optimal ascent phase. The pull-up maneuver is an additional segment of abort used to rotate the initial velocity vector and place the vehicle in a suitable direction to start optimal ascent. This is accomplished by the rapid change of a negative descent flight path angle towards a positive flight path angle ready for ascent. After the completion of the pull-up maneuver, the optimal ascent guidance (UPG+A) steers the vehicle from the end condition of the pull-up phase to the insertion into the abort orbit.

A. Pull-Up Guidance Laws

The pull-up maneuver is intended to turn around the velocity vector of the vehicle quickly during powered descent in preparation for ascent into a safe pericynthion orbit. Thus the pull-up is characterized by the change of the flight path angle from a negative value during descent to a positive targeted value at the end of the pull-up phase. The guidance strategy for this phase should focus on changing the direction of the velocity vector from a negative flight path angle during descent to a positive targeted value without significantly changing the velocity magnitude. The requirement on not causing large changes in the velocity magnitude is important because a way to change (increase) the flight path angle quickly is to reduce the velocity, which makes changing the direction of the velocity vector easier. But a lower velocity after the pull-up means more propellant is needed to increase the velocity for orbital insertion. On the other hand the velocity magnitude should not be increased significantly either in the pull-up phase because the direction of a velocity vector with a larger magnitude is more difficult to change. Therefore, objectives of the pull-up guidance are

1) Increase the flight path angle quickly from its initial (likely negative) value to a specified positive value in getting ready for ascent into the orbit
2) Cause little or no change in the magnitude of the velocity

The derivations of the following guidance laws are motivated by these two objectives. The engine thrust is always at full throttle for all the cases. The guidance laws will then determine the direction of the thrust vector.

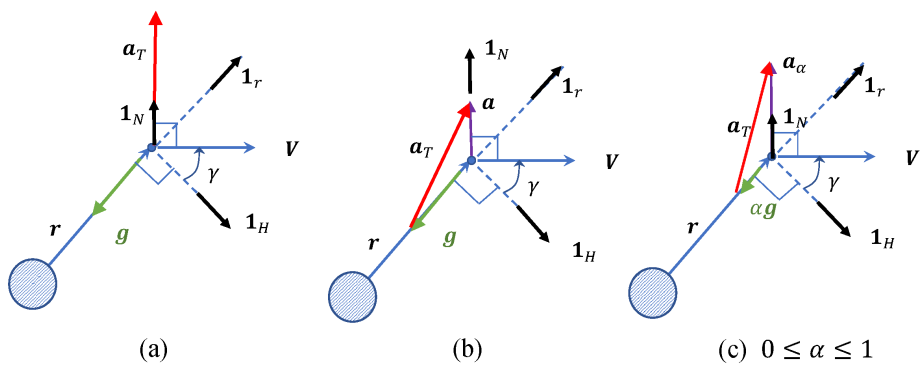

Fig. 7 Determination of the thrust acceleration vector $\boldsymbol{a}_T$ for pull-up maneuver: (a) $\boldsymbol{a}_T$ is perpendicular to the velocity vector $\boldsymbol{V}$; (b) choose the direction of $\boldsymbol{a}_T$ so that the total acceleration $\boldsymbol{a} = \boldsymbol{g} + \boldsymbol{a}_T$ is perpendicular to $\boldsymbol{V}$; (c) choose the direction of $\boldsymbol{a}_T$ so that the acceleration $\boldsymbol{a}_\alpha = \alpha\boldsymbol{g} + \boldsymbol{a}_T$ is perpendicular to $\boldsymbol{V}$

Pull-Up Guidance Law I

In this case the direction of the thrust vector is pointed upward in the vertical plane (the plane formed by the position vector $\boldsymbol{r}$ and velocity vector $\boldsymbol{V}$) and is perpendicularly to $\boldsymbol{V}$. See Figure 7(a). In this case where the full thrust vector is applied to change the direction of $\boldsymbol{V}$. Define the unit vectors

$$\mathbf{1}_r = \boldsymbol{r}/\|\boldsymbol{r}\|,\ \mathbf{1}_h = \boldsymbol{r}\times\boldsymbol{V}/\|\boldsymbol{r}\times\boldsymbol{V}\|,\ \mathbf{1}_H = \mathbf{1}_h \times \mathbf{1}_r \tag{14}$$

where $\mathbf{1}_H$ is the unit vector that defines the local horizontal direction in the vertical plane (see Fig. 7). Let γ be the flight path angle. Then the unit vector perpendicular to $\boldsymbol{V}$ and pointing upward is (cf. Fig. 7)

$$\mathbf{1}_N = \cos\gamma \mathbf{1}_r - \sin\gamma \mathbf{1}_H \tag{15}$$

The unit vector that defines the direction of the commanded thrust acceleration vector $\boldsymbol{a}_T$ then is given by the guidance law

$$\mathbf{1}_T = \mathbf{1}_N = \cos\gamma \mathbf{1}_r - \sin\gamma \mathbf{1}_H \tag{16}$$

The magnitude of $\boldsymbol{a}_T$ is $T_{max}/m(t)$ at the current time t. It should be noted that this guidance law is not the same as commanding a vertical rise where the thrust vector is always in the radial direction.

Pull-Up Guidance Law II

The direction of $\boldsymbol{a}_T$ is chosen so that the *total* acceleration vector $\boldsymbol{a} = \boldsymbol{g} + \boldsymbol{a}_T$, where $\boldsymbol{a}_T = (T_{max}/m)\mathbf{1}_T$, is perpendicular to $\boldsymbol{V}$ and pointing upward, as illustrated by Fig. 7(b). The application of the law of cosines to the triangle formed by the acceleration vectors $\boldsymbol{a}$, $\boldsymbol{g}$, and $\boldsymbol{a}_T$ in Fig. 7(b) leads to

$$a^2 + (2g\cos\gamma)a + g^2 - a_T^2 = 0 \tag{17}$$

where $a = \|\boldsymbol{a}\|$, $g = \|\boldsymbol{g}\|$, and $a_T = \|\boldsymbol{a}_T\| = T_{max}/m(t)$. For $a_T > g$ (and $|\gamma| \leq \pi/2$) this quadratic equation in a always has just one positive real root which is given by

$$a = -g\cos\gamma + \sqrt{g^2\cos^2\gamma + a_T^2 - g^2} \tag{18}$$

Clearly in this case

$$\boldsymbol{a} = a\mathbf{1}_N \tag{19}$$

Thus the commanded direction of the thrust acceleration vector is

$$\boldsymbol{a}_T = a_T\mathbf{1}_T = \boldsymbol{a} - \boldsymbol{g} \tag{20}$$

By using $\boldsymbol{g} = -g\mathbf{1}_r$, we have the guidance law for the thrust vector direction

$$\mathbf{1}_T = (g/a_T)\mathbf{1}_r + (a/a_T)\mathbf{1}_N \tag{21}$$

Because the total acceleration vector $\boldsymbol{a}$ is perpendicular to $\boldsymbol{V}$, the magnitude of the velocity vector will remain constant during the pull-up maneuver, as can be seen from the fact that

$$d\|\boldsymbol{V}\|/dt = \boldsymbol{V}^T\dot{\boldsymbol{V}}/\|\boldsymbol{V}\| = \boldsymbol{V}^T\boldsymbol{a}/\|\boldsymbol{V}\| = 0 \tag{22}$$

Pull-Up Guidance Law III

Here we develop a guidance law that is a more general form that includes both guidance laws I and II as special cases. For a specified constant α define an acceleration $\boldsymbol{a}_\alpha$

$$\boldsymbol{a}_\alpha = \alpha\boldsymbol{g} + \boldsymbol{a}_T, \quad 0 \le \alpha \le 1.0 \tag{23}$$

Again $\|\boldsymbol{a}_T\| = a_T = T_{max}/m(t)$. The direction of $\boldsymbol{a}_T$ is chosen so that the direction of $\boldsymbol{a}_\alpha$ is in the direction of $\mathbf{1}_N$. See Fig. 7(c). Similar to the derivation in guidance law II, the law of cosines gives

$$a_\alpha = -\alpha g\cos\gamma + \sqrt{\alpha^2 g^2\cos^2\gamma + a_T^2 - \alpha^2 g^2} \tag{24}$$

where $a_\alpha = \|\boldsymbol{a}_\alpha\|$. The guidance law then is

$$\mathbf{1}_T = (\alpha g/a_T)\mathbf{1}_r + (a_\alpha/a_T)\mathbf{1}_N, \quad 0 \le \alpha \le 1.0 \tag{25}$$

Evidently, when $\alpha = 0$, Guidance Law III in (25) is the same as Guidance Law I in Eq. (16); when $\alpha = 1.0$, Guidance Law III becomes Guidance Law II in Eq. (21). Hence Guidance Law III may be regarded as a nonlinear interpolation of Guidance Laws I and II over α. The presence of α offers a flexibility to adjust the guidance law for different vehicles and missions. For the vehicle model used in this paper (that of Apollo 11 Lunar Module), there is little difference for any $\alpha \in [0, 1]$, α may have more pronounced influence in other cases (especially when the thrust-to-weight ratio is low). Note that guidance laws in Eqs. (16), (21), and (25) are closed-loop guidance laws because $\mathbf{1}_r$, $\mathbf{1}_N$, a and a_α are functions of the current state.

From Eqs. (15) and (25), it is clear that the pull-up guidance laws developed here (with any $\alpha \in [0, 1]$) do not command a vertical rise – the thrust direction always has a horizontal component in the $\mathbf{1}_H$ direction unless $\gamma = 0$. If the powered descent trajectory is steep, commanding a vertical rise would kill much of the velocity of the vehicle before re-building the velocity for ascent. An extreme scenario is where the powered descent is nearly vertical. The propellant penalty of commanding a vertical rise at the beginning of abort in such a case can be non-trivial in comparison to turning the velocity vector around by the pull-up guidance law in Eq. (25) without reducing its magnitude. However, if the abort occurs right before touchdown when the lander is very close to the ground, commanding a vertical ascent is a better option because it maximizes the ground clearance during the initial part of the abort.

Under the guidance law (25), the flight path angle of vehicle will start to increase, while the velocity changes little. The pull-up phase is terminated as soon as the flight path angle reaches a prescribed targeting value of $\gamma_{end} > 0$. The attainment of the targeting condition by this simple guidance approach is guaranteed for any starting condition (that a powered descent trajectory can possibly have) and any γ_{end}, provided that the vehicle has a thrust-to-weight ratio greater than 1, a condition met by any lander. If the flight path angle is already greater or equal to γ_{end} at the start of pull-up, the pull-up phase is skipped, and the abort guidance directly enters the ascent phase. With the fuel-optimal ascent guidance and the set of orbital insertion conditions for the subsequent ascent trajectory in Section IV.A, it is found that the combined propellant usage in pull-up and ascent phases is always close to the minimum when γ_{end} has a small value, regardless where in powered descent abort is initiated. Therefore, a positive constant γ_{end} may be used. It will be shown in Section V.C that γ_{end} has a noticeable effect in overall propellant consumption in early aborts.

B. Two-Phase Abort Solutions

To facilitate the demonstration and discussion of the two-phase abort guidance results, a set of abort cases throughout powered descent are performed under the guidance. The trajectories are plotted in blue solid line in Fig. 8. The value of $\gamma_{end} = 3$ deg is used for pull-up in the simulations, unless otherwise stated. Also shown in Fig. 8 are the abort trajectories in the same cases with direct abort. Similar with the results in direct abort cases, the two-phase guidance still results in the spacecraft inserting into the target orbit at the perilune in late abort cases. However, as a result of the pull-up maneuver, in aborts between 0 and 400 seconds after PDI, the two-phase guidance strategy inserts the spacecraft into the orbit at an altitude higher than the perilune altitude, and also higher than the insertion altitudes of the direct abort trajectories, even though the spacecraft enters the same pericynthion orbit.

One of the characteristics of the pull-up maneuver is that the velocity magnitude is kept nearly constant while the flight path angle is changing from negative to positive. Figure 9 confirms the practical constancy of the velocity during the pull-up maneuver with the two-phase abort guidance. After the pull-up, the velocity is built up toward the value required to insert into the target orbit. Figure. 10 shows the changes of the flight path angle from a negative value to the specified $\gamma_{end} = 3$ deg at the end of the pull-up phase, and then along the ascent trajectory. For comparison the flight path angles for the same cases in direct abort are also plotted in Fig. 10. The pitch angle profiles in two two-phase aborts, one early and one late in the powered descent, are illustrated in Fig. 11. The pitch angles in the pull-up and ascent phases are visibly different, each accomplishing a different objective. It should be noted that the pitch angle during the ascent phase is nearly linear with respect to time, a typical characteristic of optimal ascent flight. All the 3 figures (Figs. 9–11) point to the observation that the pull-up phase is relatively short toward the end of powered descent. This is because the velocity is smaller and smaller, and turning around the flight path angle of a velocity vector with a small magnitude is quicker.

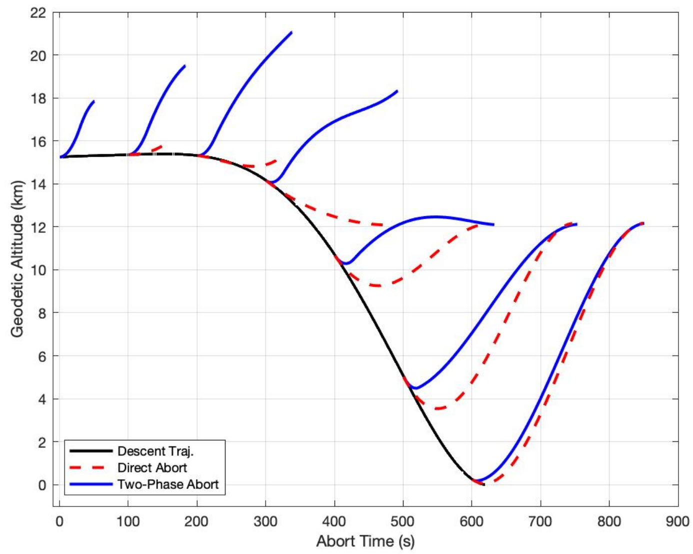

Fig. 8 Altitude comparison between direct and two-phase aborts

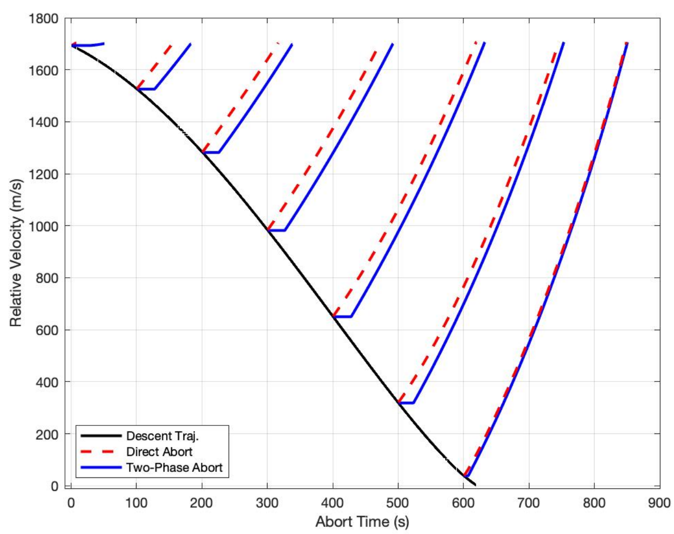

Fig. 9 Velocity comparison between direct and two-phase aborts for the cases in Fig. 8

Most importantly, the effectiveness of the two-phase guidance approach with the addition of the pull-up maneuver in ensuring safe ground clearance of the abort trajectories during late aborts is confirmed. Plotted in Fig. 12 are the abort trajectories of the same abort cases in Fig. 6, now guided by the two-phase strategy. In a sharp contrast to direct abort trajectories as seen in Fig. 6, all abort trajectories in Fig. 12 now clear the ground safely before ascending to the target orbit.

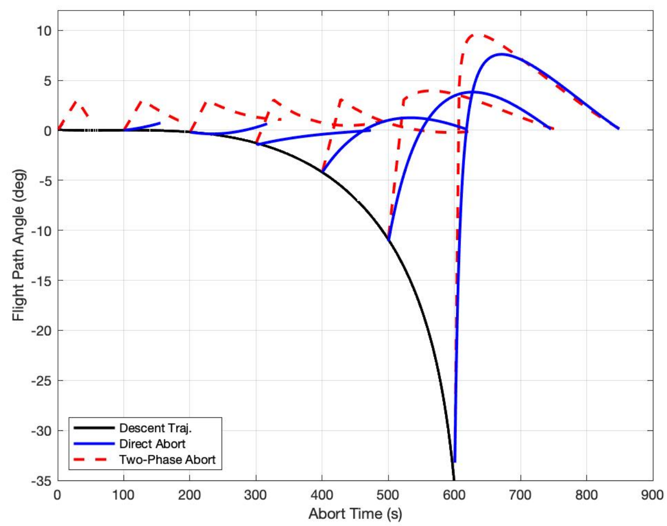

Fig. 10 Flight path angle comparison between direct and two-phase aborts for the cases in Fig. 8

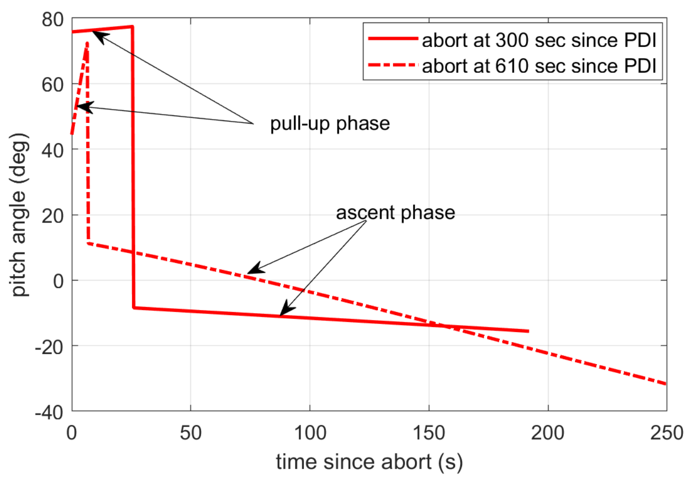

Fig. 11 Pitch angles in early and late aborts

C. Effects of the Parameter γ_{end} in Pull-Up Maneuver

Direct abort under UPG+A is propellant optimal. The two-phase guidance is propellant optimal from the exit of pull-up to orbital insertion. But how does the total fuel consumption from both phases of the abort compare to the optimal value? The answer depends on the value of γ_{end}, the target flight path angle that defines the end of the pull-up maneuver. Table 3 summarizes the propellant consumption for several abort cases taking place at points from early in powered descent to near touchdown with direct abort and two-phase abort. Two different values of γ_{end} are used in the closed-loop simulations, 3.0 deg and 0.1 deg, respectively. For γ_{end} = 3.0 deg, the propellant usage by the two-phase guidance approach is noticeably higher than that by direct abort for early aborts. But the difference shrinks as abort occurs later in powered descent, to the point of practically nonexistent toward the end.

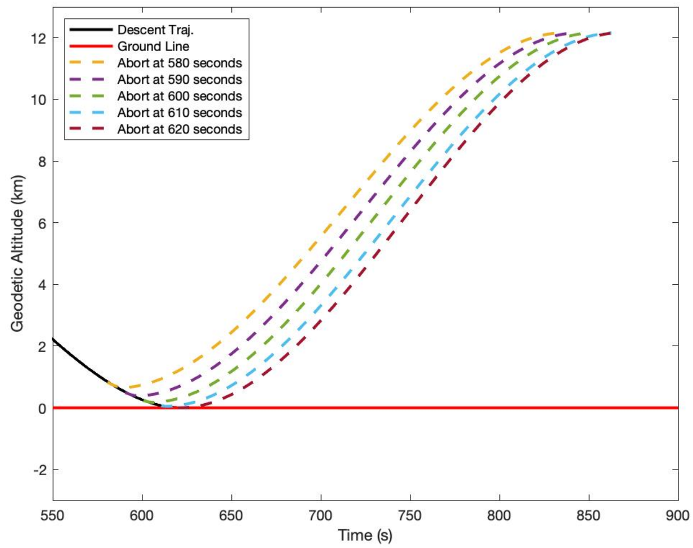

Fig. 12 Late abort solutions using two-phase abort guidance; ground clearance is achieved

Table 3 Propellant consumption comparison between direct and two-phase abort

Abort Time (s)	Total Propellant Consumption (kg)		
	Direct Abort	Two-Phase Abort (γ_{end} = 3 deg)	Two-Phase Abort (γ_{end} = 0.1 deg)
100	808.58	1209.95	820.76
200	1709.74	2021.44	1738.65
300	2546.47	2821.90	2632.29
400	3224.36	3420.66	3332.84
500	3619.76	3730.45	3703.49
600	3665.82	3687.72	3685.21

On the other hand, if γ_{end} = 0.1 deg is used, late abort trajectories still clear the ground, and the propellant consumption by the two-phase abort guidance approach comes very close to the overall optimal values (by direct abort) throughout the powered descent phase, as can be seen in Table 3. This is not a surprise though. Recall that the pull-up guidance law is developed with the realization that using the thrust vector to only change the direction of the velocity vector in pull-up phase should be fuel efficient. Here we have demonstrated that with an appropriate choice of γ_{end} (likely a small positive value), the overall propellant consumption of the two-phase guidance strategy is near optimal. Hence the proposed two-phase guidance approach not only effectively addresses the ground clearance concerns, but also can be made achieve practically minimum propellant usage.

Figure 13 depicts the abort trajectories with γ_{end} = 0.1 deg and γ_{end} = 3 deg starting from the same conditions at several points along the powered descent trajectory. Figure 14 compares the flight path angles in these trajectories.

From these two figures it clear that the two-phase abort trajectories with $\gamma_{end} = 0.1$ are quite close to the direct abort trajectories in the same cases as seen in Figs. 8 and 10. This explains the near-optimal propellant usages of two-phase aborts with $\gamma_{end} = 0.1$ as given in Table 3.

Figures 13 and 14 indicate the effects of γ_{end} are more pronounced in early aborts. But for late aborts, the effects of different values of γ_{end} gradually diminish, eventually to a negligible level. If necessary, a predefined table of γ_{end} as a function of the abort time since PDI may be loaded into the guidance system to provide a means for shaping the abort trajectory.

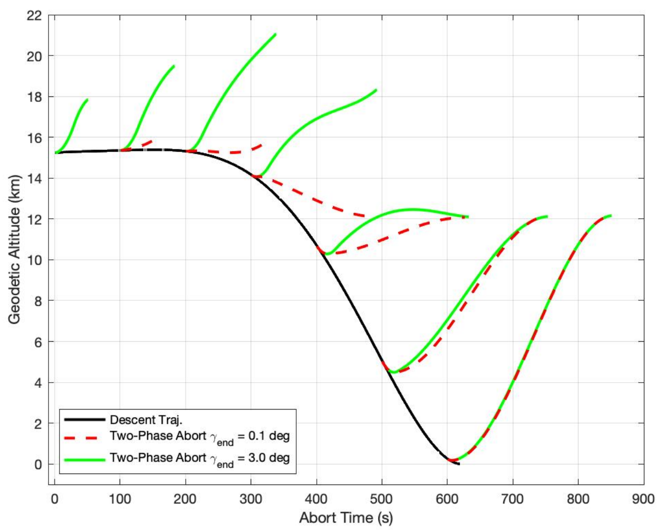

Fig. 13 Ascent trajectory comparison for two-phase abort with two different flight-path-angle γ_{end} in pull-up maneuver

VI. Monte Carlo Testing of Two-Phase Abort Guidance

To gain a thorough assessment of the performance and reliability of the two-phase abort guidance method, Monte Carlo closed-loop simulations are performed. The abort time is randomly chosen between 0 and 610 sec since PDI in each Monte Carlo simulation, signifying the fact that abort can happen at any moment throughout the powered descent. We note that the initial condition for an abort would be different even at the same time since PDI, depending on the actual powered descent trajectory because it is also subject to dispersions and uncertainty. To create dispersed powered descent trajectories, the initial condition of the powered descent trajectory is dispersed randomly, resulting different powered descent trajectory in each case. Furthermore, the initial mass of the vehicle and the actual engine thrust are also dispersed, and the actual values are not known to the guidance system. Table 4 shows the distributions and 3-sigma/min-max values of the dispersions. These values represent “nominal dispersions", and they correspond to a factor of safety (FOS) of 1.0. The FOS is essentially a scaling factor. At FOS of 2.0, all the 3-sigma values in

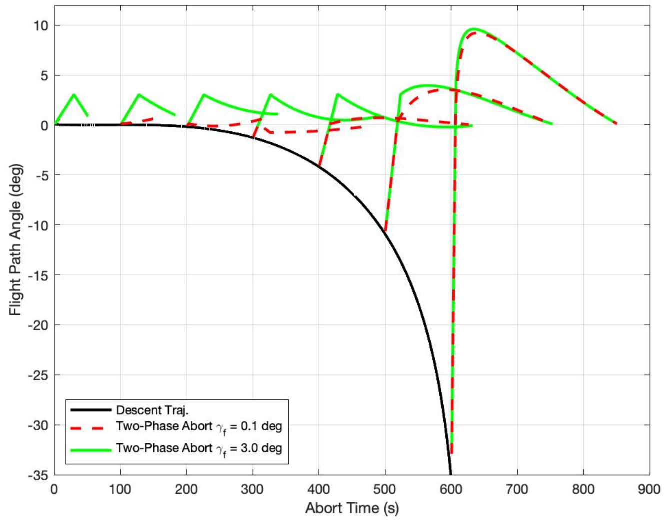

Fig. 14 Flight path angle comparison for two-phase abort with two different flight-path-angle γ_{end} in pull-up maneuver

Table 4 will be doubled (the range of variations of the abort time is not affected by FOS), FOS of 5.0 leads to 5 times as large dispersions, and so on and so forth. Therefore a larger value of FOS stresses the guidance system more. All the dispersions except for the abort time are Gaussian with a zero mean. The abort time is dispersed as a uniform distribution to simulate the fact that abort can happen at any time during the powered descent.

Table 4 Dispersions used in Monte Carlo simulations at FOS = 1.0

parameter	distribution	3-sigma (or [min, max])
PDI altitude (m)	zero-mean, Gaussian	100
PDI longitude (deg)	zero-mean, Gaussian	0.25
PDI latitude (deg)	zero-mean, Gaussian	0.25
PDI velocity (m/s)	zero-mean, Gaussian	3.3
PDI flight path angle (deg)	zero-mean, Gaussian	0.1
PDI azimuth angle (deg)	zero-mean, Gaussian	0.17
PDI mass (kg)	zero-mean, Gaussian	49.84
engine thrust (N)	zero-mean, Gaussian	450.0
abort time (s)	Uniform	$[0, 610]$

With the dispersions in Table 4, 3000 dispersed at runs at FOS=1.0 were made under the proposed two-phase abort guidance method. Figure 15 shows the 3000 abort trajectories during powered descent. Table 5 lists statistics in the orbital insertion conditions, propellant usages, and ascent times of the 3000 trajectories. Note that the specified orbital insertion conditions are the eccentricity (0.0385), semi-major axis (1818.1 km) and inclination (90 deg) of the final orbit. Table 4 indicates that the specified final orbit was accurately achieved in all cases. On the other hand, the insertion

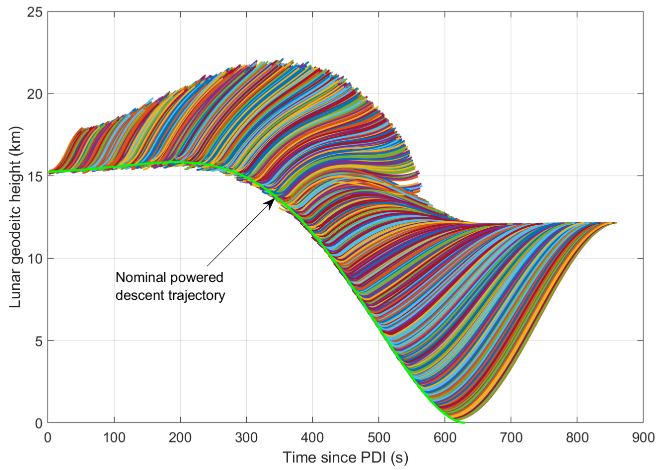

Fig. 15 3000 Monte Carlo abort trajectories (FOS=1.0)

altitude, velocity, and flight path angle are not specified and they are dependent on where the ascent trajectory enters the target orbit (therefore the data in Table 4 on these quantities do not reflect any measure of accuracy). The statistics on the insertion mass in the table show that in the worst case, the insertion mass was 4,698 kg, still more than the dry mass of the vehicle of 4,479 kg as given in Table 1. This suggests that there was still about 200 kg of propellant left at the orbital insertion, even in the worst case. But this relatively small margin also highlights the importance for the guidance to fly fuel-optimal ascent trajectory as UPG+A does.

Figure 16 shows the spread of the true anomalies at the orbital insertion along the 3000 trajectories. It can be seen that earlier aborts entered the target orbits after the perilune, with true anomaly as large as 30 deg; late aborts entered the target orbit pre-perilune with negative true anomalies. When the aborts occurred after 500 sec since PDI, the abort trajectories inserted right at perilune with a zero true anomaly. There are a few cases for abort at about 210 sec that appear to have out-of-pattern true anomalies. These cases will be investigated later in detail.

Table 5 Statistics of orbital insertion conditions in 3000 Monte Carlo simulations at FOS = 1.0

parameter	mean	standard deviation	max	min
ascent time (s)	1.5283E+02	7.2254E+01	2.4315E+02	2.0748E+01
altitude (km)	1.4431E+01	3.9175E+00	2.0029E+01	1.0003E+01
velocity (m/s)	1.7020E+03	3.6722E+00	1.7062E+03	1.6967E+03
flight path angle(deg)	5.5749E-01	5.2055E-01	1.1383E+00	-8.9695E-01
eccentricity	3.8500E-02	1.9880E-06	3.8586E-02	3.8436E-02
semi-major axis (km)	1.8181E+03	3.7472E-03	1.8183E+03	1.8180E+03
inclination (deg)	9.0000E+01	0.0000E+00	9.0000E+01	9.0000E+01
propellant usage (kg)	2.2549E+03	1.0661E+03	3.5876E+03	3.0613E+02
insertion mass (kg)	9.1603E+03	3.0610E+03	1.4386E+04	4.6981E+03
abort time (s)	3.0698E+02	1.7438E+02	6.0987E+02	2.0829E-01

Next, to further stress the abort guidance by creating more significantly different initial conditions of aborts and

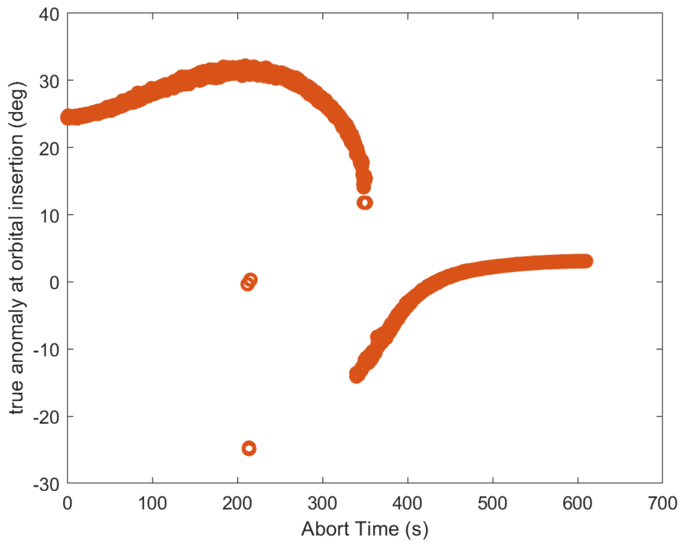

Fig. 16 True anomalies of 3000 trajectories at orbital insertion(FOS=1.0)

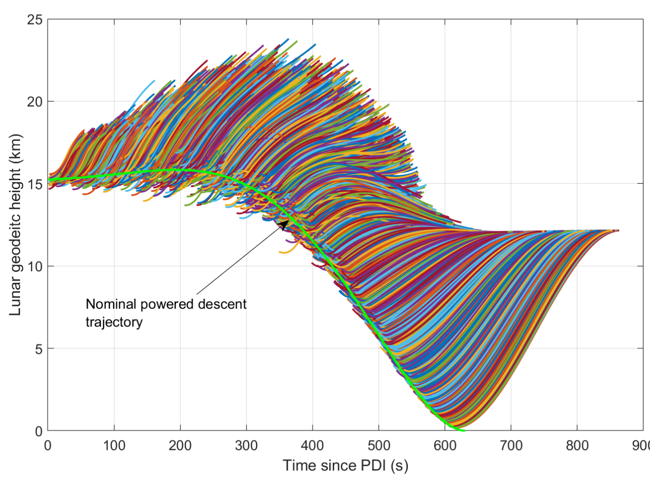

Fig. 17 3000 Monte Carlo abort trajectories (FOS=5.0)

larger uncertainty, 3000 Monte Carlo simulations were performed at FOS=5.0, that is, with 5 times the dispersions in Table 4. Figure 17 shows the 3000 dispersed abort trajectories. The effects of significantly larger dispersions are clearly visible as compared to Fig. 15. The fact that many of the abort trajectories in Fig. 17 started noticeably away from the nominal powered descent trajectory is because the actually dispersed powered descent trajectories (where the aborts started) were significantly off from the nominal powered descent trajectory at FOS of 5.0. In contrast to Fig. 15, Fig. 17 also points to large spread of orbital insertion conditions due to the dispersions of 5 times compared at FOS=1.0.

Table 6 contains the statistics of the orbital insertion conditions in these cases. It is evident from the table that the orbital insertion conditions on eccentricity, semi-major axis, and inclination were still accurately attained. The orbital

Table 6 Statistics of orbital insertion conditions in 3000 Monte Carlo simulations at FOS = 5.0

parameter	mean	standard deviation	max	min
ascent time (s)	1.5288E+02	7.2334E+01	2.4839E+02	2.0850E+01
altitude (km)	1.4409E+01	3.9265E+00	2.1700E+01	1.0003E+01
velocity (m/s)	1.7020E+03	3.6807E+00	1.7066E+03	1.6952E+03
flight path angle(deg)	5.4801E-01	5.2773E-01	1.2216E+00	-9.5137E-01
eccentricity	3.8501E-02	1.0953E-05	3.9099E-02	3.8499E-02
semi-major axis (km)	1.8181E+03	2.0722E-02	1.8192E+03	1.8181E+03
inclination (deg)	9.0000E+01	0.0000E+00	9.0000E+01	9.0000E+01
propellant usage (kg)	2.2557E+03	1.0673E+03	3.6649E+03	3.0764E+02
insertion mass (kg)	9.1586E+03	3.0642E+03	1.4481E+04	4.5200E+03
abort time (s)	3.0698E+02	1.7438E+02	6.0987E+02	2.0829E-01

insertion altitude (which is not constrained) has a significantly large spread as compared to the cases with FOS=1.0. Figure 18 confirms this observation with the plot of the orbital insertion altitudes versus abort time for both FOS=1.0 and FOS=5.0. The much larger spread for FOS=5.0 is unmistakable. A manifestation of significantly larger dispersions is wider variations of propellant usage as evidenced in Fig. 19. In the worst case (with the smallest insertion mass) the propellant mass used was only about 40 kg less than the total propellant carried as given in Table 1, meaning that there was little propellant margin left at FOS of 5.0. Nonetheless, the abort guidance held up really well even in the presence of very large dispersions at FOS of 5.0, guiding every single abort trajectory successfully into the specified target orbit.

Figures 20 and 21 illustrate the histograms of the instants when aborts happened during the powered descent along the 3000 trajectories, and the times of flight for ascent into the target orbit. As expected, the abort times were distributed uniformly throughout the powered descent as they were so implemented in the Monte Carlo simulations. The ascent times in more cases appear to cluster around the high end of 240 sec than other values, perhaps a reflection of a nonlinear correlation between the abort times and ascent times.

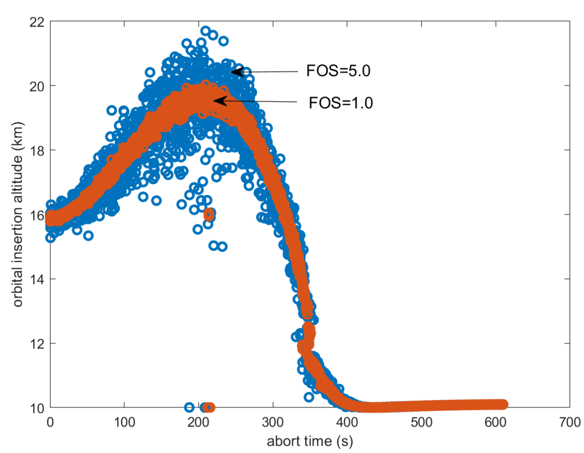

Fig. 18 Orbital insertion altitudes (FOS=1.0 and 5.0, respectively)

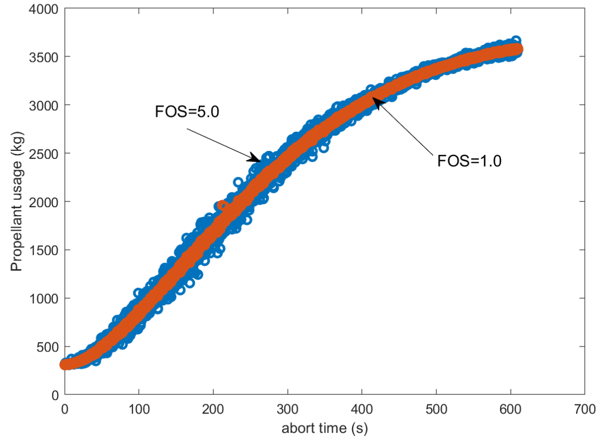

Fig. 19 Propellant usages in aborts (FOS=1.0 and 5.0, respectively)

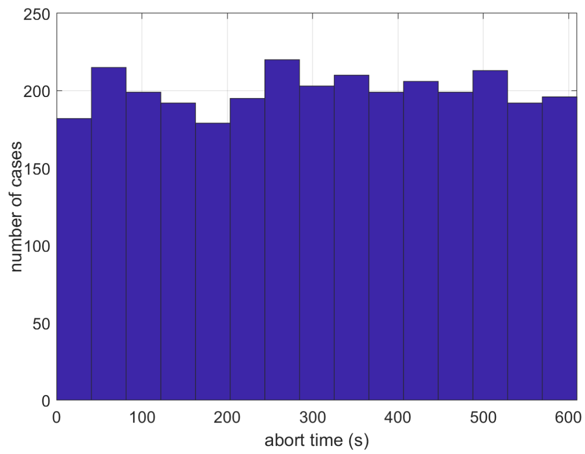

Fig. 20 Uniform distribution of abort times in powered descent

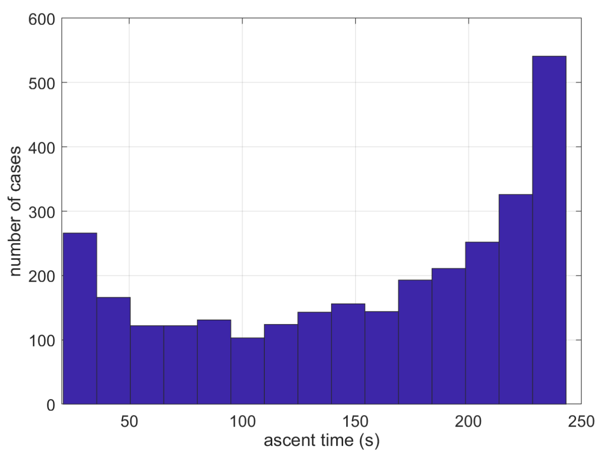

Fig. 21 Ascent times along abort trajectories

VII. Multiple Optima in Abort Ascent

During the course of investigation, a peculiar phenomenon is observed in some of the abort ascent trajectories. There are some cases that appear as outliers to the pattern of their neighboring ascent trajectories. We see a few such cases in Fig. 16 where the true anomalies at orbital insertion are noticeably different from others. As another evidence, Fig. 22 shows 3000 abort trajectories at different times along the nominal powered descent trajectory (there are no dispersions in the PDI condition, initial mass, and thrust magnitude included in these 3000 cases). It can be seen that a cluster of cases at about 200 s end at altitudes notably lower than the orbital insertion altitudes of the adjacent ascent trajectories. At first glance, it seems that these "out-of-family" cases failed to meet the terminal conditions. But a closer look shows that each of these trajectories still successfully delivers the vehicle to the specified final orbit. The lower insertion altitudes in these cases arise as the insertion true anomalies have different values and sign as compared to others (on the opposite side of perilune of the target orbit), as seen in Fig. 23. Figure 24 on the other hand indicates that the propellant usages for these out-of-family cases do not appear to be out of line with respect to the neighboring trajectories. The question left unanswered is why UPG+A guides these cases to clearly different insertion points. A complete understanding of the reason is important because the confidence in the abort guidance strategy and guidance algorithm is at stake.

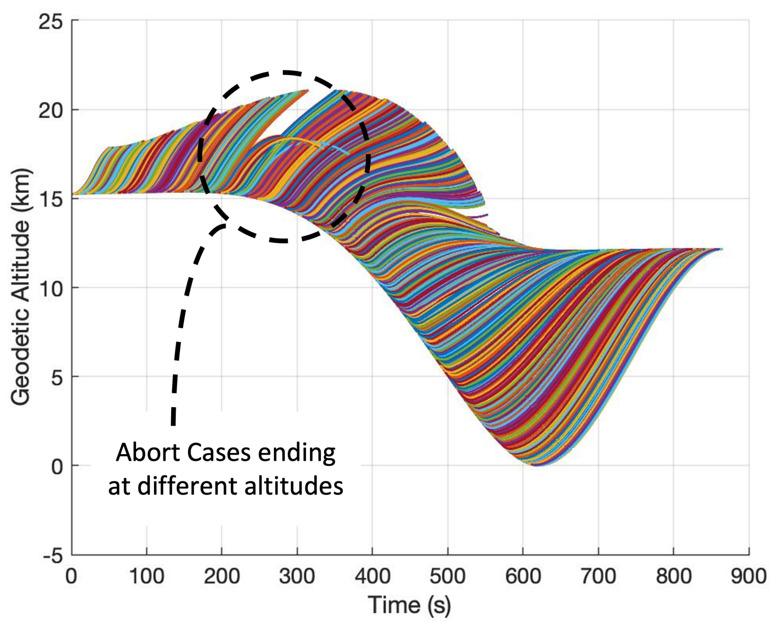

Fig. 22 Abort trajectories throughout powered descent: notice the outlier cases ending at different altitudes

To investigate the root cause of this mystery, the following approach is taken: at each given abort time along the powered descent trajectory, initiate the abort by first executing the pull-up maneuver. Starting from the condition at the end of the pull-up maneuver, solve the fuel-optimal ascent problem to insert the target orbit at a specified point, as opposed to the free-attachment-point case. In other words, the terminal constraints for the optimal ascent problem are

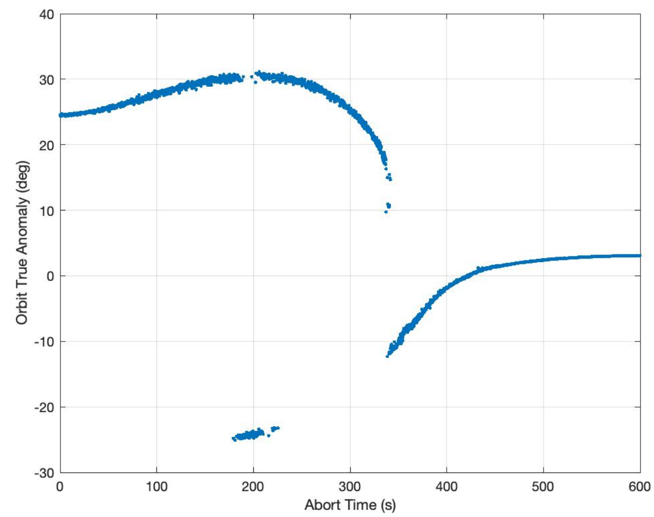

Fig. 23 True anomalies at orbital insertion points for the 3000 abort cases in Fig. 22

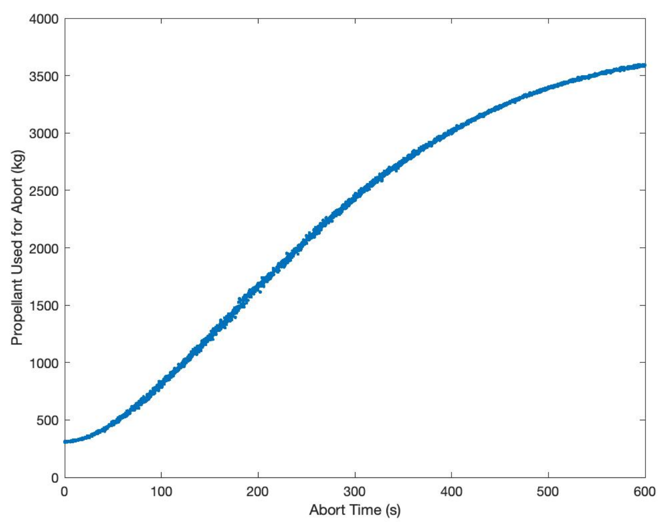

Fig. 24 Propellant consumption by the 3000 abort cases in Fig. 22

those on the semi-major axis (a), eccentricity (e), orbital inclination (i), *and* true anomaly. Then for the same initial condition of optimal ascent and the same a, e, and i, a range of values for the insertion true anomaly are scanned. The corresponding propellant consumption from this true-anomaly sweep are recorded and plotted. The curve so obtained represents the optimal propellant consumption for a particular abort case when the orbital insertion point is varied along the target orbit. This problem is solved independently using both UPG+A (recall that UPG+A can accommodate any combination of orbital insertion conditions) and OpenMDAO. The solutions yielded by the two methods are the same.

Figure 25 depicts such curves for 8 abort cases along the nominal powered descent trajectory at different times, 100 s apart, from 150 s since PDI to 500 s since PDI. Each curve in Fig. 25 represents the variation of the optimal propellant consumption with respect to the insertion true anomaly for an abort with the same initial conditions. The different points on a particular curve provides the optimal propellant usage corresponding to different orbital insertion points into the same orbit.

Figure 25 reveals that for early aborts (before 350 s since PDI), in each curve, there is local minimum and a global minimum for the optimal propellant consumption, one on each side of the perilune (where the true anomaly is zero). The geometric interpretation of the two trajectories inserting at the local and global optima is illustrated in Fig. 26. The global minimum appears to favor a positive true anomaly. Further analysis shows that the global minimum is always associated with a higher insertion altitude than the local minimum, but the propellant consumption differs by a very small amount (which is also evident from Fig. 25). Figure 25 also shows that as the abort occurs later, the local and global optima gradually merge into one, and there is only one global optimum which is moving closer to the perilune. This observation explains why for the late aborts the orbital insertion altitudes in Fig. 22 are close to the perilune altitude and the true anomalies in Fig. 23 are close to zero.

Now we have a convincing answer to the question posed at the beginning of this section. The reason why in some cases the ascent trajectory ends at a different altitude, as seen in Fig. 22, is that the guidance algorithm (UPG+A) converges to the local optimum of the free-attachment-point instead of the global minimum. This explains the out-of-family cases in Fig. 22. It should be pointed out that the possibility of convergence to a local optimum is not a unique issue for UPG+A, but a common trait shared by all deterministic optimization methods for non-convex problems. We used OpenMDAO for the same aborts cases between 200 and 300 s after PDI, and some of them (not necessarily the same cases) also converged to the local minimum. Since the optimal propellant consumption is very close, entering the target orbit at an insertion point that represents the local optimum carries no practical drawbacks and poses no risk to the safety of the abort. Therefore the seemingly out-of-family ascent trajectories seen in Fig. 22 are not a cause for any concerns. If there are additional considerations, such as for rendezvous with a rescue vehicle already on a lunar orbit, that constrain where the vehicle should insert into the target orbit, UPG+A remains applicable as soon as the targeting condition is specified.

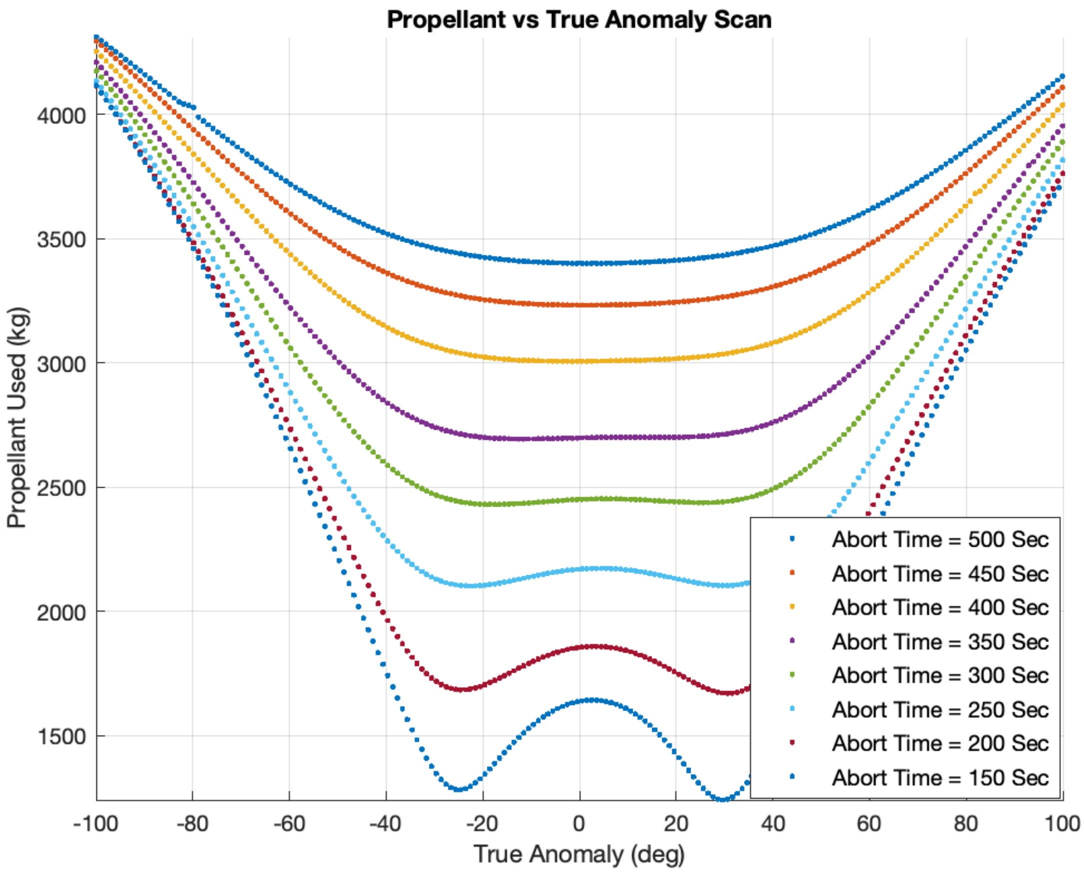

Fig. 25 Optimal propellant consumption in abort-ascent for insertion into different points on the target orbit

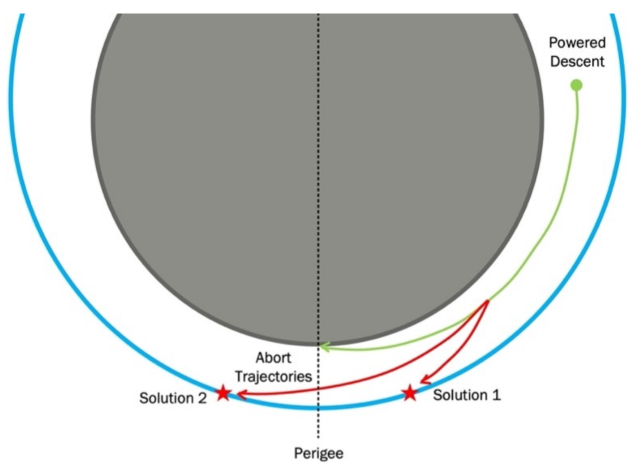

Fig. 26 Two optimal insertion points into the same target orbit, one local minimum (Solution 1), the other global minimum (Solution 2)

VIII. Conclusions

This work represents a first focused effort in public domain since the Apollo program on developing guidance strategy and method for abort during powered descent of a crewed lunar mission. The problem is to autonomously guide the lander during powered descent to abort the landing mission when necessary, and ascend safely to a specified clear pericynthion orbit. The problem is challenging because the initial condition of the abort can be drastically different, depending on where the abort takes place on the descent trajectory. And the initial condition can be very “unnatural" for ascent flight - the flight path angle can have a negative value of large magnitude. In this paper, a novel two-phase abort strategy and associated guidance law and algorithm are developed. Once abort is commenced, the vehicle is first steered to pull up from descent while keeping the velocity magnitude constant to reach a state that ensures ground clearance and is amendable to ascent flight. Then a fuel-optimal ascent guidance algorithm guides the vehicle to accurately insert into the target abort orbit. This strategy is simple and clean and the guidance is fully automated, free of complex flight-condition dependent logic. The operation is fully adaptive, requiring no extensive pre-mission planning or pre-loaded nominal guidance sequences, and capable to execute abort at any point on the powered descent trajectory where abort is still physically feasible. The validity of the guidance solution is verified independently by a different method. Parametric studies show that the total propellant consumption achieved by the two-phase guidance approach can be made practically the same as that of the complete fuel-optimal abort solution, but the two-phase strategy eliminates the risk of ground collision. The effectiveness and robustness of the proposed method are demonstrated in this paper by extensive closed-loop simulations with a baseline crewed landing mission at the South Pole of the Moon.

This paper does not address other considerations such as post-abort rendezvous and rescue maneuvers. But the methodology is flexible and adaptive to any feasible abort condition and targeting condition that is achievable, hence such considerations can be integrated into the guidance solution by simply specifying appropriate targeting conditions for aborts at different times.

Acknowledgments

The authors at San Diego State University would like to thank the support to this research by the NASA Space Technology Research Fellowship 80NSSC18K1170 and the NASA Cooperative Agreements 80NSSC19M0119 and 80NSSC21M0342.

References

[1] Hyle, C. T., Foggatt, C. E., and Webber, B. D., "Apollo Experience Report - Abort Planning," NASA TN D-6847, 1972.

[2] Kurten, P. M., "Apollo Experience Report - Guidance and Control Systems: Lunar Module Abort System," NASA TN D-7990, 1975.

[3] Bennett, F. V., "Apollo Experience Report – Mission Planning for Lunar Module Descent and Ascent," NASA TN D-6846, 1972.

[4] Goodman, J. L., "Powered Guidance Development for Apollo and the Space Shuttle," AAS Paper 16-093, 2016.

[5] Scofield, H. N., "A simplified explicit guidance scheme for orbital injection." *Journal of Spacecraft and Rockets*, Vol. 5, No. 11, 1968, pp. 1309–1311. https://doi.org/10.2514/3.29474.

[6] Lu, P., and Sandoval, S. A., "Abort Guidance during Powered Descent for Crewed Lunar Missions," AIAA Paper 2021-0505, 2021. https://doi.org/10.2514/6.2021-0505.

[7] Lu, P., Griffin, B. J., Dukeman, G. A., and Chavez, F. R., "Rapid Optimal Multiburn Ascent Planning and Guidance," *Journal of Guidance, Control, and Dynamics*, Vol. 31, No. 6, 2008, pp. 1656–1664. https://doi.org/10.2514/1.36084.

[8] Sandoval, S. A., Lu, P., Hwang, J. T., Rea, J. R., and Sostaric, R. R., "Multiple Optima in Abort Ascent during Lunar Powered Descent," AIAA Paper 2022-0949, 2022. https://doi.org/10.2514/6.2022-0949.

[9] Sandoval, S. A., and Lu, P., "Powered Descent Guidance for a Crewed Lunar Landing Mission," *AAS Guidance and Control Conference, Breckenridge, CO*, AAS Paper 20–044, 2020.

[10] Lu, P., "Theory of Fractional-Polynomial Powered Descent Guidance," *Journal of Guidance, Control, and Dynamics*, Vol. 43, No. 3, 2020, pp. 398–409. https://doi.org/10.2514/1.G004556.

[11] Klumpp, A. R., "Apollo Lunar Descent Guidance," *Automatica*, Vol. 10, No. 2, 1974, pp. 133–146. https://doi.org/10.1016/0005-1098(74)90019-3.

[12] Cherry, G. W., "A General, Explicit, Optimizing Guidance Law for Rocket-Propelled Spaceflight," AIAA Paper 64-638, 1964. https://doi.org/10.2514/6.1964-638.

[13] Lu, P., "Propellant-Optimal Powered Descent Guidance," *Journal of Guidance, Control, and Dynamics*, Vol. 41, No. 4, 2018, pp. 813–826. https://doi.org/10.2514/1.G003243.

[14] Pontryagin, L. S., Boltyanskii, V. G., Gramkreledze, Q. V., and Mishchenko, E. F., *The Mathematical Theory of Optimal Processes*, Intersciences, New York, 1962, Chap. 3.

[15] Pan, B., Chen, Z., Lu, P., and Gao, B., "Reduced Transversality Conditions in Optimal Space Trajectories," *Journal of Guidance, Control, and Dynamics*, Vol. 36, No. 5, 2013, pp. 1289–1300. https://doi.org/10.2514/1.60181.

[16] Gray, J. S., Hwang, J. T., Martins, J. R. R. A., Moore, K. T., and Naylor, B. A., "OpenMDAO: An open-source framework for multidisciplinary design, analysis, and optimization," *Structural and Multidisciplinary Optimization*, Vol. 59, No. 4, 2019, pp. 1075–1104. https://doi.org/10.1007/s00158-019-02211-z.